Article

TRANSPARENT PROCESS

EMBO reports

Extended synaptotagmin regulates membrane contact site structure and lipid transfer function *in vivo*

Vaisaly R Nath[1,2], Shirish Mishra[1], Bishal Basak[1], Deepti Trivedi[1] & Padinjat Raghu[1,*]

Abstract

Inter-organelle communication between closely apposed membranes is proposed at membrane contact sites (MCS). However, the regulation of MCS structure and their functional relevance *in vivo* remain debated. The extended synaptotagmins (Esyt) are evolutionarily conserved proteins proposed to function at MCS. However, loss of all three Esyts in yeast or mammals shows minimal phenotypes questioning the functional importance of Esyt. We report that in *Drosophila* photoreceptors, MCS number is regulated by PLCβ activity. Photoreceptors of a null allele of *Drosophila* extended synaptotagmin *(dEsyt)* show loss of ER-PM MCS. Loss of dEsyt results in mislocalization of RDGB, an MCS localized lipid transfer protein, required for photoreceptor structure and function, ultimately leading to retinal degeneration. *dEsyt* depletion enhanced the retinal degeneration, reduced light responses and slower rates of plasma membrane PIP_2 resynthesis seen in *rdgB* mutants. Thus, dEsyt function and PLCβ signaling regulate ER-PM MCS structure and lipid transfer in *Drosophila* photoreceptors.

Keywords *Drosophila*; ER-PM contact sites; extended synaptotagmins; lipid transfer; PIP_2 signaling

Subject Categories Membrane & Trafficking

DOI 10.15252/embr.202050264 | Received 20 February 2020 | Revised 12 June 2020 | Accepted 22 June 2020 | Published online 27 July 2020

EMBO Reports (2020) 21: e50264

Introduction

One of the key attributes of eukaryotic cells is the existence of membrane bound organelles each with its own unique protein and lipid composition. The role of vesicular transport between organelles in establishing and maintaining this composition is well accepted. However, it has also been observed that in intact cells, organelle membranes are often placed in close proximity to each other without undergoing fusion as described for vesicular transport. This concept of closely apposed organelle membranes is referred to as Membrane Contact Sites (MCS) that are now defined as sites where organelle membranes are found separated by a gap of 10–30 nm. MCS were noted in the electron microscopy studies of George Palade (Palade & Porter, 1957), and subsequent studies have described MCS in several cell types (Carrasco & Meyer, 2011; Hayashi *et al*, 2008; Hepler *et al*, 1984; Suzuki & Hirosawa, 1994). The endoplasmic reticulum (ER), the largest organelle in the cell, forms an elaborate tubular network that occupies much of the interior of the cell and therefore establishes MCS with most other organelles (Gatta & Levine, 2017) including the plasma membrane (PM). A number of molecular processes are proposed to occur at MCS; these include Ca^{2+} homeostasis, lipid transfer between organelle membranes, and signaling interactions between proteins located at membranes on either side of the MCS [reviewed in refs. Saheki and De Camilli (2017), Balla *et al* (2019)]. However, the mechanisms by which MCS are established and maintained as well as their importance for cell physiology *in vivo* remain unclear.

Every organelle has a unique lipid composition that is a critical determinant of its function. Since lipids are hydrophobic and cannot diffuse in aqueous cytosol, lipid composition depends on the transport of lipid to and away from organelle membranes. Such intracellular lipid trafficking is mediated both by vesicular transport and by the activity of lipid transfer proteins (LTP). A major function that has been proposed for MCS is the activity of LTP at these sites, and several studies have demonstrated that LTPs can be localized to membrane contact sites [reviewed in ref. Cockcroft and Raghu (2018)]. Thus, the integrity of MCS is likely to be central to lipid homeostasis in eukaryotic cells. However, the depletion of multiple proteins localized to MCS and is thought to contribute to their structure and functions have showed limited effect on cell physiology, questioning the relevance, and importance of MCS function for lipid homeostasis *in vivo*.

Membrane contact sites between the PM and the ER are found in many cell types. Studies in yeast have shown that a major fraction of the ER shows a cortical localization (Pichler *et al*, 2001) and is confined in close proximity to the PM. The ER and PM have distinct lipid compositions; the ER is a major site of lipid biosynthesis, and multiple lipids including phosphatidylinositol are enriched in this

1 National Centre for Biological Sciences-TIFR, Bangalore, India
2 School of Biotechnology, Amrita Vishwa Vidyapeetham, Amritapuri, Kollam, Kerala, India
*Corresponding author. Tel: +91 080 2366 6001; E-mail: praghu@ncbs.res.in

compartment. By contrast, the PM is enriched in distinct lipid classes including phosphatidylinositol 4,5-bisphosphate (PIP_2) and phosphatidylinositol 4-phosphate (PI4P) that are not found at the ER membrane. Remarkably, the PI4P phosphatase Sac1 is localized at the ER while its substrate PI4P is enriched at the PM. Elegant studies in yeast have proposed that Sac1 is localized to ER-PM MCS and functions to dephosphorylate PI4P in *trans* (Stefan *et al*, 2011). Proteomic studies in yeast have identified a set of 6 proteins, referred to as tethers that interact with Sac1 and are localized to ER-PM contact sites. These include Scs2 and Scs22 (VAP orthologs; Loewen *et al*, 2007), Ist2 (member of TMEM16 ion channel family; Manford *et al*, 2012), and the tricalbin proteins (Tcb1, Tcb2, Tcb3—Esyt orthologs; Manford *et al*, 2012). Depletion of all these proteins using a so-called *Δtether* strain leads to the collapse of the cortical ER (cER) away from the PM and elevated PI4P levels at the PM (Manford *et al*, 2012). However, the *Δtether* strain shows remarkably mild phenotypes, with only a limited change in PM permeability described on heat stress (Omnus *et al*, 2016) raising the question of whether the presence of contact sites are required to support cell physiology.

Extended synaptotagmins (Esyts) are a group of ER anchored proteins belonging to the tubular lipid binding (TULIP) superfamily that comprise an N-terminal transmembrane domain, a synaptotagmin like mitochondrial lipid binding protein domain (an SMP domain) and several acidic phospholipid binding C2 domains that bind to PM lipids (Chang *et al*, 2013). Mammalian cells have three independent genes that encode for Esyt: *Esyt1, Esyt2* and *Esyt3*. Studies in mammalian cells have described localization of these proteins to ER-PM contact sites and proposed a role for Esyt in mediating lipid transfer function (Giordano *et al*, 2013). It has been proposed that Ca^{2+} and PIP_2 mediate the localization and tethering of Esyt to ER-PM contact sites (Bian *et al*, 2018; Yu *et al*, 2016) and that this is linked to the lipid transfer activity of the SMP domain (Idevall-hagren *et al*, 2015; Yu *et al*, 2016). Thus, two independent roles have been proposed for Esyt: one as a member of a group of proteins that function as a tether at ER-PM contact sites and another as a lipid transfer protein via its SMP domain. Yet, the yeast *Δtether* strain that lacks all Esyt genes shows remarkably mild phenotypes (Omnus *et al*, 2016). A triple knockout of mouse *Esyt1, Esyt2* and *Esyt3* is viable and shows no major changes in brain morphology, synaptic protein composition, and stress response (Sclip *et al*, 2016). Even so, another *in vitro* study on $Esyt2^{-/-}/Esyt3^{-/-}$ mouse embryonic fibroblast cells exhibit declined migratory potential and are vulnerable to stressed culture conditions (Herdman *et al*, 2014) questioning the role of Esyts in supporting function *in vivo*. Interestingly, in *Drosophila*, Esyt is reported to be localized to the presynaptic compartment in the neuromuscular junction and implicated in regulating neurotransmitter release and synaptic growth (Kikuma *et al*, 2017). Therefore, the *in vivo* function of this highly conserved protein family and the role of Esyt in supporting contact site functions remain unresolved.

In *Drosophila* photoreceptors, sensory transduction is mediated by G protein-coupled phospholipase C mediated PIP_2 turnover (Raghu *et al*, 2012). The biochemical reactions that constitute the PIP_2 cycle in these cells are organized around an ER-PM contact site between the sub-microvillar cisternae (SMC), a specialized compartment of the ER and the microvillar PM (reviewed in ref. Yadav *et al*, 2016). Localized to this contact site is a multi-domain protein retinal degeneration B (RDGB) that includes an N-terminal phosphatidylinositol transfer domain (PITP) that can transfer PI and PA i*n vitro*; binding of PI to the PITP domain is essential for the *in vivo* function of RDGB (Yadav *et al*, 2015). Loss of this function in flies lacking RDGB protein results in key *in vivo* phenotypes: reduced electrical response to light (reduction in ERG amplitude), delay in PIP_2 resynthesis, and light-dependent degeneration of photoreceptors (retinal degeneration) (reviewed in ref. Cockcroft *et al*, 2016). Thus, *Drosophila* photoreceptors offer an ideal *in vivo* model to test the mechanisms that control ER-PM contact site structure and lipid transfer. In this study, we have generated a loss-of-function mutant for the only Esyt in *Drosophila* and studied its phenotypes in photoreceptors. We find that PLCβ-dependent Esyt function is required to support ER-PM contact site structure as well as the lipid transfer function of RDGB *in vivo*.

Results

A single gene encodes for Esyt in *Drosophila*

Bioinformatic analysis revealed that the *Drosophila* genome encodes a single ortholog of human Esyt and the tricalbin proteins of yeast (Fig 1A). The *Drosophila* extended synaptotagmin gene (*dEsyt*) is CG6643 located on the third chromosome (cytolocation 96A7-96A7). *dEsyt* encodes for four different transcripts: RA, RB, RC, and RD that are identical except for a 75 bp sequence between the 2nd and 3rd C2 domain coding regions where each isoform has different sequences. Sequence comparison for all four transcripts showed that the RA CDS is the shortest, lacking 100 nucleotides at the 5′ end and the RD transcript specifically lacks 9 nucleotides which encode for 3 amino acid residues that are identical in the other three transcripts. When aligned with human Esyt1 (GI: 296317244), CG6643 shows 93% query coverage and 35% sequence identity with all four isoforms. The protein domain structure of dEsyt is conserved with that of the human and yeast orthologs (Fig 1B). For, e.g., in hEsyt proteins, a single N-terminal SMP domain and multiple C2 domains are described. dEsyt sequence shows the presence of an SMP domain and three C2 domains. This feature along with the conserved interdomain distance makes dEsyt most similar to hEsyt2 and hEsyt3. Transcriptome analysis indicates that *dEsyt* is ubiquitously expressed across tissues and during all developmental stages (http://flybase.org/reports/FBgn0266758). However, qPCR analysis showed that *dEsyt* transcripts are enriched in the head compared to the body (Fig 1C). To determine whether dEsyt expression is enriched in the eye, we made use of so^D (Roederer *et al*, 2005), a dominant allele of the *sine oculis* gene that results in a block in eye development and eliminates eye tissue. If a given gene is enriched in the eye, transcript expression is expected in wild-type heads but will be reduced in so^D heads since eye tissue, where the gene is mainly expressed is missing. For *dEsyt*, a comparison between transcript expression in wild-type and so^D heads shows similar levels of expression, suggesting that RNA for this gene is not enriched in the eye (Fig 1D).

dEsyt is dispensable for normal phototransduction

To examine a possible function of *dEsyt*, a null allele was generated using CRISPR/Cas9-based genome editing (Kondo & Ueda, 2013;

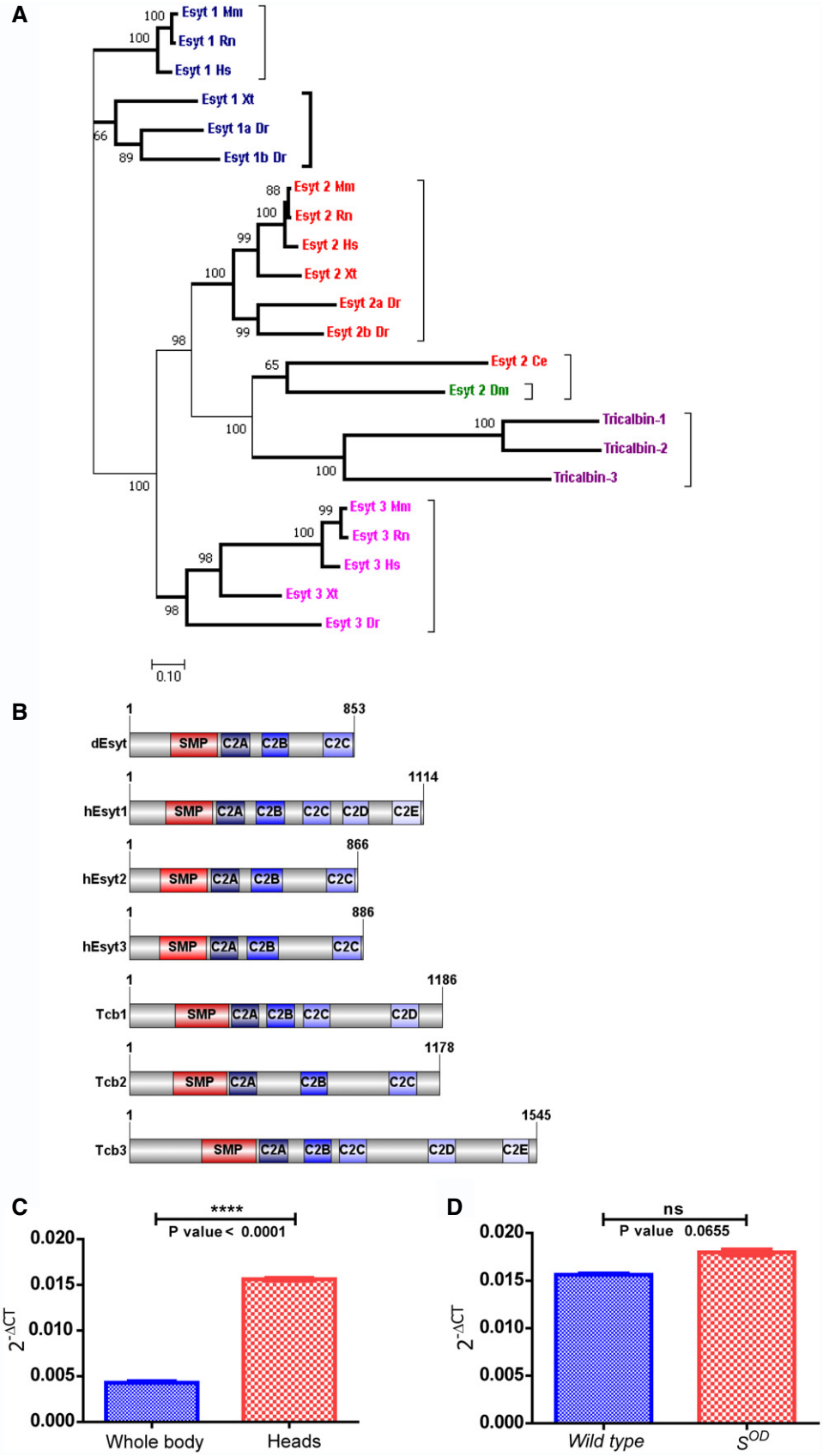
A
Esyt 1 Mm
Esyt 1 Rn
Esyt 1 Hs
Esyt 1 Xt
Esyt 1a Dr
Esyt 1b Dr
Esyt 2 Mm
Esyt 2 Rn
Esyt 2 Hs
Esyt 2 Xt
Esyt 2a Dr
Esyt 2b Dr
Esyt 2 Ce
Esyt 2 Dm
Tricalbin-1
Tricalbin-2
Tricalbin-3
Esyt 3 Mm
Esyt 3 Rn
Esyt 3 Hs
Esyt 3 Xt
Esyt 3 Dr
0.10
B
dEsyt
hEsyt1
hEsyt2
hEsyt3
Tcb1
Tcb2
Tcb3
SMP
C2A
C2B
C2C
C2D
C2E
C
****
P value < 0.0001
2-ΔCT
Whole body
Heads
D
ns
P value 0.0655
Wild type
SOD

Figure 1.

Figure 1. Single gene encoding Esyt expressed in *Drosophila melanogaster*.

A Schematic showing the phylogeny of extended synaptotagmin in different organisms: *Drosophila melanogaster* (Dm), *Saccharomyces cerevesiae* (Tricalbin), *Homo sapiens* (Hs), *Mus Musculus* (Mm), *Rattus norvegicus* (Rn), *Caenorhabditis elegans* (Ce), *Danio rerio* (Dr), and *Xenopus tropicalis* (Xt). Bold lines—subnodes. Numbers on the nodes—bootstrap value. Colors—Esyt1, Esyt2, and Esyt3 clusters.

B Schematic of dEsyt-PA protein domain structure aligned with mammalian Esyts and yeast tricalbins (Image generated using IBS, Illustrator for Biological sciences, version 1.0 software http://ibs.biocuckoo.org/) (Liu *et al*, 2015). Amino acid numbers in each protein are indicated. SMP-SMP domain. C2A, B, C, D, and E are the various C2 domains.

C Quantitative real-time PCR analysis showing head enrichment of *dEsyt*; the *X*-axis indicates the wild-type tissues from which RNA was isolated, and *Y*-axis indicates the *dEsyt* transcript-level expression normalized to the loading control (RP49-ribosomal protein 49), $n = 3$ replicates (biological).

D Quantitative real-time PCR analysis showing *dEsyt* transcript-level expression in head RNA samples from wild-type and s^{OD}. *Y*-axis indicates the *dEsyt* transcript-level expression normalized to the loading control (RP49-ribosomal protein 49), $n = 3$ replicates (biological).

Data information: Bar graphs with mean ± SD are shown. Statistical tests: (C and D) Student's unpaired *t*-test (two-tailed). ns—Not significant. ****$P < 0.0001$.

Appendix Method S1). The resulting genome edit deleted the nucleotide sequence corresponding to 488 amino acids of the dEsyt coding region; this was verified using molecular techniques (Refer to Appendix Fig S1). During larval development, $dEsyt^{KO}$ homozygous larvae show a delay in development and adult flies that eclose are smaller than controls (Appendix Fig S2A and B). These phenotypes can be rescued by pan larval reconstitution with *dEsyt* cDNA (Appendix Fig S2C and D). Although most $dEsyt^{KO}$ homozygotes do not eclose as adults, when grown on nutrient-enriched medium, a small proportion is viable as homozygous adults.

To test the potential role of *dEsyt* in supporting lipid transfer at MCS, we studied the phenotypes of these homozygous $dEsyt^{KO}$ in adult photoreceptors. We measured electrical responses to light in adult flies. Electroretinograms (ERG) were recorded from wild-type and $dEsyt^{KO}$ adults of matched age and eye color. We found that the absolute ERG response of $dEsyt^{KO}$ was smaller than that of controls (Fig 2A). However, the ERG response is an extracellular recording that scales with the size of the eye. Since $dEsyt^{KO}$ are smaller in size than controls, we normalized the raw ERG response of each animal to its body size (Fig 2B); this normalized ERG amplitude was not significantly different between control and $dEsyt^{KO}$.

Since contact sites are proposed to support lipid transfer reactions during cell signaling, we tested the requirement for dEsyt in supporting PIP_2 turnover during phototransduction. We compared the level of PIP_2 at the microvillar PM of photoreceptors in wild-type and $dEsyt^{KO}$ flies. To monitor the changes in the PIP_2 levels, the PH domain of PLCδ fused to GFP (hereafter referred to as PH-GFP) was utilized (Yadav *et al*, 2015). This analysis revealed no difference in the basal levels of PIP_2 between controls and $dEsyt^{KO}$ (Fig 2C). Further, following bright light stimulation to activate PLCβ and deplete PIP_2 at the microvillar PM, we found no difference in the rate at which PIP_2 levels were restored at the microvillar PM (Fig 2D and E) in $dEsyt^{KO}$. Similarly, the P4M-GFP probe was utilized to monitor the levels of PI4P which acts as the substrate for *dPIP5K* to produce PIP_2 (Balakrishnan *et al*, 2018); basal PI4P levels and PI4P turnover kinetics were similar between wild-type and $dEsyt^{KO}$ (Appendix Fig S3A, B and E).

Light-dependent retinal degeneration is a common outcome when genes essential for phototransduction are disrupted (Raghu *et al*, 2012). To test the role if any, of *dEsyt* in regulating phototransduction, we monitored the integrity of rhabdomere (apical PM) structure following illumination. Although normal at eclosion, when flies were grown under constant bright illumination, normal photoreceptor ultrastructure was retained until 10 days post-eclosion. However, photoreceptors of $dEsyt^{KO}$ underwent progressive retinal degeneration when observed till day 16 with substantial loss of rhabdomere integrity (Fig 2F and G). This light-dependent degeneration exhibited by the mutant *dEsyt* homozygotes was rescued by reconstitution with wild-type dEsyt transgene (Fig 2H).

Loss of dEsyt enhances $rdgB^9$ phenotypes

It is reported that mammalian Esyt1 enhances the activity of Nir2 by recruiting it to the ER-PM junctions subsequent to an elevation in cytosolic calcium levels (Chang *et al*, 2013). We tested the function of dEsyt in supporting the activity of RDGB, the *Drosophila* ortholog of Nir2. For this, we generated a double-mutant strain of $dEsyt^{KO}$ with $rdgB^9$, a hypomorphic allele of *rdgB* ($rdgB^9;dEsyt^{KO}$). Using this strain, we compared the impact of *dEsyt* deletion on the phenotypes of the $rdgB^9$ single mutant.

In *Drosophila*, *rdgB* mutants show a number of key phenotypes including light-dependent retinal degeneration, reduced electrical response to light, and altered PIP_2 homeostasis at the microvillar PM (Yadav, et al. 2015). We compared the time course of retinal degeneration in $rdgB^9$ v $rdgB^9;dEsyt^{KO}$ and noted that $dEsyt^{KO}$ accelerates the time course of retinal degeneration in $rdgB^9$ (Fig 3Ai, ii and 3B). Over this time period, $dEsyt^{KO}$ itself does not show any retinal degeneration; the retinal degeneration of the $dEsyt^{KO}$ occurs much later after eclosion.

We also studied the ERG amplitude in response to a 1 s flash of light. As previously reported (Yadav *et al*, 2015), $rdgB^9$ mutants show a reduced ERG amplitude and this was further reduced in $rdgB^9;dEsyt^{KO}$ (Fig 3C and D). Finally, we measured PIP_2 levels at the microvillar PM under resting conditions. The PIP_2 levels in $rdgB^9$ are lower than in wild type (Yadav et al, 2015), but there was no difference in resting PIP_2 levels between $rdgB^9$ and $rdgB^9;dEsyt^{KO}$ (Fig 3F). However, when we measured the rate of recovery of microvillar PIP_2 following its depletion by strong PLCβ activation, the reduced rate of PIP_2 recovery in $rdgB^9$ was further delayed in $rdgB^9;dEsyt^{KO}$ (Fig 3E and G) and a similar observation was also made for PI4P levels (Appendix Fig S3C–E). Collectively, loss of *dEsyt* worsened the three key functional and biochemical outcomes in a hypomorphic allele of *rdgB*.

dEsyt is localized to ER-PM contact sites in photoreceptors

To understand the mechanism by which loss of dEsyt enhances $rdgB^9$ phenotypes, it was crucial to decipher the localization of

dEsyt. Since Esyt proteins have been described as components of MCS in both yeast and mammalian cells, we tested whether the same is also true in *Drosophila* photoreceptors. For this, we labeled wild-type retinae with anti-dEsyt serum (Kikuma *et al*, 2017). Single confocal images of photoreceptor cross-sections (R1–R6) revealed a crescent-shaped distribution of dEsyt at the MCS between the microvillar PM and the SMC (Fig 4A); this staining was absent in *dEsyt*^{KO} photoreceptors demonstrating the specificity of the labeling detected. To further confirm this observation, we expressed dEsyt tagged to the fluorescent protein mCherry in photoreceptors and examined its localization using an antibody against mCherry; here too we found that dEsyt::mCherry was localized to the MCS at the base of the microvilli in photoreceptors (Fig 4B); staining was not seen in wild-type photoreceptors not expressing dEsyt::mCherry

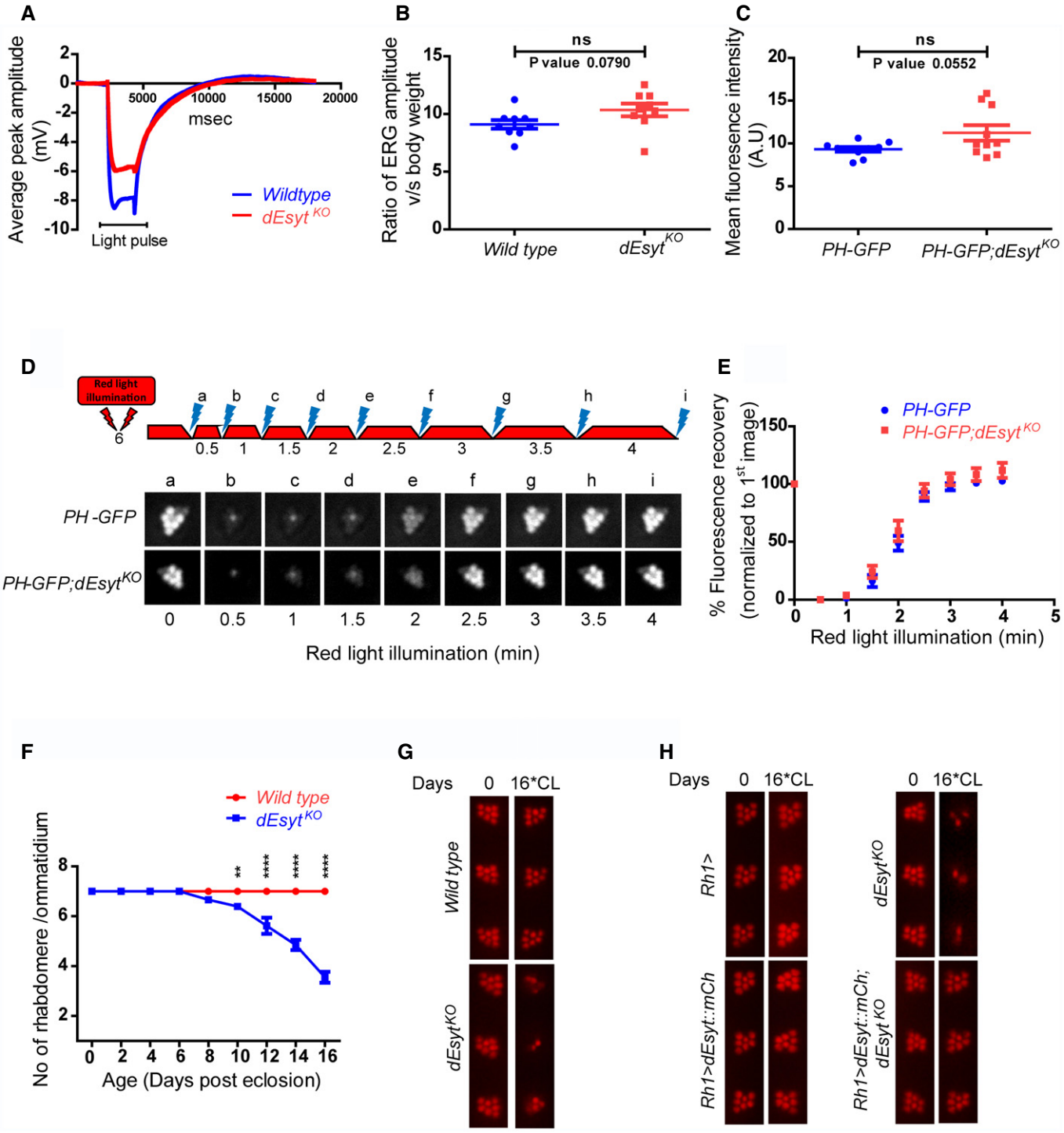

Figure 2.

Figure 2. *dEsyt* is dispensable for phototransduction.

A Representative ERG trace from dark reared 0 to 1-day-old flies of the indicated genotype stimulated by 2-s flash of green light. The duration of the stimulating light is shown. *Y*-axis shows the amplitude of the ERG response. *X*-axis shows the duration of the recording.

B Graph showing ERG amplitude normalized to body weight. *Y*-axis shows the ratio of ERG amplitude of individual flies to their body weight. *X*-axis indicates genotypes. Each data point represents an individual fly tested. Error bar represents s.e.m.

C Quantification of the mean fluorescence intensity of the deep pseudopupil formed by the PIP_2 probe PH-GFP in the one-day-old flies of the indicated genotypes (n = 10 biological replicates).

D Deep pseudopupil imaging of PIP_2 levels in the microvillar membrane of photoreceptors. The fluorescence of the PH-GFP probe is depicted. The protocol used is shown with red light illumination periods shown as red bars and flashes of blue light (a–f) used for image capture depicted. Representative deep pseudopupil images acquired at specified time points are depicted. Genotypes as indicated.

E Graph quantifying the recovery kinetics of the fluorescent pseudopupil with time, *X*-axis represents the genotypes, *Y*-axis represents intensity normalized to the intensity of the first image (n = 10 biological replicates). Error bars represent s.e.m.

F Quantification of the time course of retinal degeneration. 10 ommatidia from 5 separate flies of each genotype were scored and plotted. *Y*-axis is the number of intact rhabdomeres/ommatidium. The maximum value possible is 7. *X*-axis is the age of the flies post-eclosion.

G Representative optical neutralization (ON) images showing rhabdomere integrity of the indicated genotypes. Rearing conditions and the age of the flies are indicated on top (*CL-constant light).

H Representative ON images showing the rescue of rhabdomere structural integrity in $dEsyt^{KO}$ mutants on expressing the dEsyt::mCherry transgene. Genotypes of the flies are indicated on the left. Rearing conditions and the age of the flies are indicated on top.

Data information: Scatter plots and XY plots with mean ± SD are shown. Statistical tests: (B and C) Student's unpaired *t*-test. (E and F) Two-way ANOVA grouped analysis with Bonferroni post-tests to compare replicate means. ns—Not significant; $^{**}P < 0.01$; $^{****}P < 0.0001$.

indicating the specificity of the staining. Collectively, these findings demonstrate that dEsyt is localized at the ER-PM MCS in photoreceptors.

dEsyt function is required to localize RDGB to ER-PM contact sites

One mechanism by which loss of *dEsyt* might enhance $rdgB^9$ phenotypes is by reducing the levels of the endogenous RDGB protein. We checked the levels of RDGB protein in $dEsyt^{KO}$ mutants exposed to bright light illumination for increasing time intervals and found that the RDGB protein levels remain unaltered even after retinal degeneration is initiated in $dEsyt^{KO}$ (Fig 4C). A second mechanism could be the mislocalization of the RDGB protein away from the ER-PM MCS. In wild-type *Drosophila* photoreceptors, RDGB is strictly localized to the MCS and we found that this localization was not disrupted in newly eclosed $dEsyt^{KO}$ flies (Fig 4D). However, when exposed to constant illumination for 6 days post-eclosion, $dEsyt^{KO}$ photoreceptors showed mislocalization of RDGB away from the MCS; the protein was now diffused across the photoreceptor cell body (Fig 4E). By contrast, under the same conditions, RDGB localization to the MCS was retained in wild-type photoreceptors (Fig 4E). Thus, dEsyt function is required for the normal localization of RDGB at the MCS in photoreceptors.

dEsyt is necessary for PLCβ-dependent modulation of ER-PM MCS

The most direct way of assessing MCS structure is by transmission electron microscopy (TEM). We used fixation methods that allow enhanced membrane preservation and better visualization of membranes and MCS (Matsumoto-Suzuki *et al*, 1989; Fig 5A i, ii); in addition to the membranes seen, the perfectly spherical black bead-like structures in the micrographs are pigment granules. Such images allowed us to quantify the fraction of PM at the base of the microvilli that was in contact with the SMC (hereafter referred to as MCS density) in each ultrathin section of a photoreceptor. On day 1 after eclosion, in the light-sensitive R1-R6 photoreceptors of dark-reared wild-type flies, the MCS density was ca. 50% (Fig 5A i, ii, and 5B i). As flies aged, the MCS density decreased to ca. 30% by day 14 (Fig 5A iii, iv, and 5B i). Under the same conditions, the MCS density in the UV-sensitive R7 photoreceptor remained constant as a function of age (Fig 5B ii); this serves as an internal control for phenotypes directly linked to illumination since the light used for our illumination experiments contains visible wavelengths but not those in the ultraviolet range. We also measured the MCS density in the $norpA^{P24}$ mutant allele that lacks PLCβ protein expression (Pearn *et al*, 1996). MCS density in $norpA^{P24}$ was ca. 30% at eclosion (Fig 5C i, ii) but in contrast to wild-type flies, $norpA^{P24}$ flies did not show any reduction as a function of age; i.e., 14-day-old $norpA^{P24}$ photoreceptors showed the same MCS density as wild-type cells at eclosion (Fig 5D i). Thus, MCS density in photoreceptors is dependent on age and PLCβ activity.

To assess the contribution of dEsyt to ER-PM MCS structure, we performed TEM on $dEsyt^{KO}$ photoreceptors to visualize and quantify MCS density (Fig 5E iii, iv). At eclosion, MCS density was not different between wild-type and $dEsyt^{KO}$ for R1-R6 photoreceptors (Fig 5E i–iv and 5F i); a similar result was seen in UV-sensitive R7 photoreceptors (Fig 5F ii). Thus, loss of dEsyt does not impact the establishment of ER-PM contact sites during development in *Drosophila* photoreceptors. We then examined MCS density as a function of age in $dEsyt^{KO}$ (Fig 6A i–iv). While MCS density was reduced from ca. 50% (day 1) to 30% at day 14 in wild-type flies (Fig 5B i), in $dEsyt^{KO}$ flies, the number of MCS was reduced to almost none by day 14 (Fig 6B i). By contrast, in UV-sensitive R7 photoreceptors, MCS density was only modestly reduced in $dEsyt^{KO}$ (Fig 6B ii).

We tested the impact of PLCβ activity on the enhanced loss of MCS in $dEsyt^{KO}$. For this, we compared MCS density in $dEsyt^{KO}$ with that in the $norpA^{P24}$;$dEsyt^{KO}$ double mutant (Fig 6C i–iv). Strikingly, the absence of basal PLCβ activity in $norpA^{P24}$;$dEsyt^{KO}$ photoreceptors completely rescued MCS number in 14-day-old flies; this was in sharp contrast to $dEsyt^{KO}$ flies which at this stage typically shows very few or no MCS (Fig 6C iii, iv, and 6D i). Thus, the loss of MCS in $dEsyt^{KO}$ with age depends on ongoing PLCβ activity.

We also examined MCS structure in $rdgB^9$ photoreceptors (Fig 6E i, ii). In dark-reared flies, just after eclosion, MCS density in R1-R6 photoreceptors was already reduced significantly (Fig 6F i). $rdgB^9$;

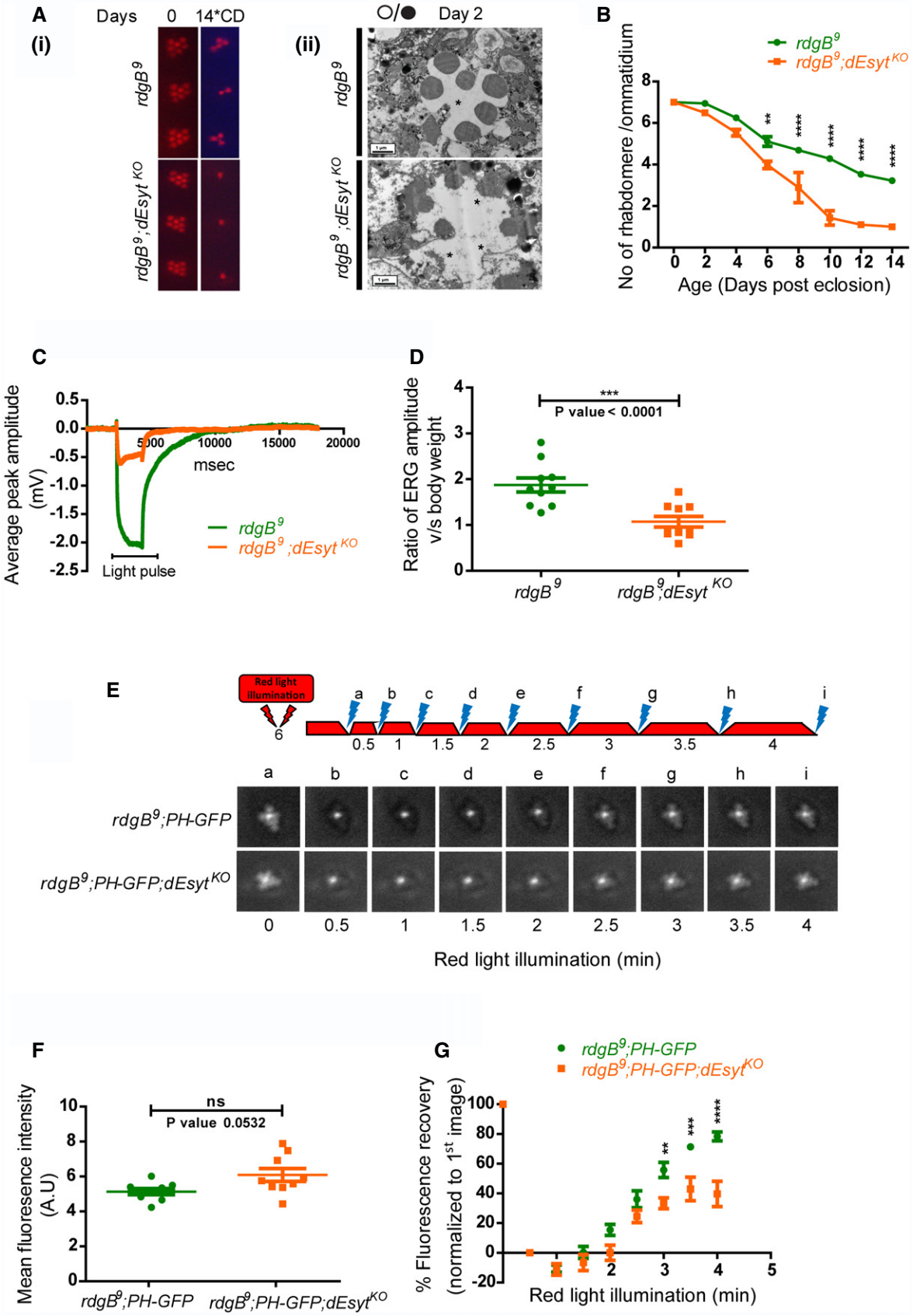
A
(i)
Days 0 14*CD
rdgB9
rdgB9;dEsyt KO
(ii)
Day 2
rdgB9
rdgB9;dEsyt KO
B
rdgB9
rdgB9;dEsyt KO
No of rhabdomere /ommatidium
Age (Days post eclosion)
C
Average peak amplitude (mV)
msec
Light pulse
rdgB9
rdgB9;dEsyt KO
D
Ratio of ERG amplitude v/s body weight
P value < 0.0001
rdgB9
rdgB9;dEsyt KO
E
Red light illumination
rdgB9;PH-GFP
rdgB9;PH-GFP;dEsyt KO
Red light illumination (min)
F
Mean fluorescence intensity (A.U)
ns
P value 0.0532
rdgB9;PH-GFP
rdgB9;PH-GFP;dEsyt KO
G
rdgB9;PH-GFP
rdgB9;PH-GFP;dEsyt KO
% Fluorescence recovery (normalized to 1st image)
Red light illumination (min)

Figure 3.

Figure 3. Loss of *dEsyt* enhances *rdgB* mutant phenotypes.

A (i) Representative optical neutralization (ON) images showing rhabdomere structure of the indicated genotypes. Rearing conditions and the age of the flies are indicated on top (*CD-constant dark). (ii) TEM images showing a single ommatidium from the photoreceptors of $rdgB^{9}$ and $rdgB^{9}$;$dEsyt^{KO}$ mutants reared in 12-h L/D cycle for 2 days. Scale bar: 1 μm (asterisk indicates degenerated rhabdomere).

B Quantification of the time course taken for retinal degeneration. 10 ommatidia were scored from 5 flies of each genotype and plotted.

C Representative ERG traces showing the duration of light pulse, *X*-axis indicates time in msec, and *Y*-axis indicates the average ERG amplitude in mV.

D Graph showing ERG amplitude of $rdgB^{9}$ and $rdgB^{9}$;$dEsyt^{KO}$ normalized to body weight. *Y*-axis shows the ratio of ERG amplitude of individual flies to their body weight. *X*-axis indicates genotypes. Each data point represents an individual fly tested. Error bar represents s.e.m.

E Deep pseudopupil imaging of PIP_2 levels in the microvillar membrane of photoreceptors. The fluorescence of the PH-GFP probe is depicted. The protocol used is shown with red light illumination periods shown as red bars and flashes of blue light (a–f) used for image capture depicted. Representative deep pseudopupil images acquired at specified time points are depicted. Genotypes as indicated.

F Quantification of the mean fluorescence intensity of the PIP_2 probe PH-GFP from the deep pseudopupil formed by one-day-old flies of the indicated genotypes (n = 10 biological replicates).

G Graph quantifying the recovery kinetics of the fluorescent pseudopupil with time, *X*-axis represents the genotypes, and *Y*-axis represents intensity normalized to the intensity of the first image (n = 10 biological replicates).

Data information: Scatter plots and XY plots with mean ± SD are shown. Statistical tests: (D and F) Student's unpaired *t*-test. (B and G) Two-way ANOVA grouped analysis with Bonferroni post-tests to compare replicate means. ns—Not significant; $^{**}P < 0.01$; $^{***}P < 0.001$; $^{****}P < 0.0001$.

$dEsyt^{KO}$ photoreceptors also showed very few MCS in the photoreceptors (Fig 6E iii,iv); these were quantified only from photoreceptors in which there was minimal degeneration of rhabdomeres (Fig 6E iii). Further, $rdgB^{9}$;$dEsyt^{KO}$ double mutants showed substantially greater rhabdomeral degeneration than $rdgB^{9}$ (Fig 3A ii) when reared for 2 days under conditions of 12-h L/D cycle reflecting the ultrastructural level observations seen in the optical neutralization assays (Fig 3B).

Discussion

Studies in yeast and mammalian cells have identified proteins that when overexpressed, localize to ER-PM MCS. However, in most cases, surprisingly, loss of function of these proteins appears to not impact cellular function or *in vivo* physiology. Though Esyt can localize to ER-PM MCS in cultured mammalian cells (Chang *et al*, 2013; Giordano *et al*, 2013), depletion of Esyt in cultured mammalian cells apparently does not impact cell physiology and knockout of Esyt in mice does not have discernible impact on animal physiology (Sclip *et al*, 2016; Tremblay & Moss, 2016) raising questions on their role *in vivo*. However, in this study, we found that a null mutant of the only Esyt in *Drosophila* showed developmental delay (data not shown), reduced adult viability and homozygotes that eclosed were smaller than controls; the reduced body size could be rescued by reconstitution with a wild-type transgene suggesting an important role for *dEsyt* in growth. While the cellular and molecular basis of these phenotypes remains to be established, these data clearly demonstrate a function for Esyt in supporting animal physiology *in vivo*.

Importantly, we analyzed photoreceptor structure and function in $dEsyt^{KO}$ since this cell type critically depends on lipid transfer activity at its ER-PM MCS for phototransduction (Yadav *et al*, 2016, 2018). In newly eclosed $dEsyt^{KO}$ flies, photoreceptor ultrastructure was unaffected and ER-PM MCS density was not different from that in wild-type flies. Thus, dEsyt is not required during development to establish ER-PM MCS. We also found that $dEsyt^{KO}$ showed normal electrical responses to light and basal levels of PM PI4P and PIP_2 as well as their turnover during PLCβ signaling was unaffected; this finding implies that dEsyt function is dispensable for PIP_2 turnover (that in turn depends on PI transfer at ER-PM MCS) during PLCβ signaling. Our observation is consistent with that reported for mammalian Esyt that the SMP domain does not exhibit specific PI transfer activity *in vitro* (Saheki *et al*, 2016; Schauder *et al*, 2014), that loss of Esyt function in cultured mammalian cells does not impact PIP_2 turnover during PLCβ signaling, and that depletion of Esyt does not impact store-operated calcium influx, a key output of PLCβ activation (Giordano *et al*, 2013).

Despite the apparent lack of a phenotype in $dEsyt^{KO}$ photoreceptors, we found that loss of dEsyt enhances all three key phenotypes of $rdgB^{9}$, a hypomorphic allele with ca. 5% residual RDGB protein in photoreceptors. Importantly, the impact of $dEsyt^{KO}$ on the reduced light response and PM PIP_2 levels in $rdgB^{9}$ occurred in newly eclosed flies, prior to the onset of retinal degeneration. Conceptually, this enhancement could be due to a change in the levels of the major phototransduction proteins but this was ruled out since we found no alteration in the levels of these proteins (Rhodopsin, PLC, Gq, and TRP) in $rdgB^{9}$;$dEsyt^{KO}$ (Appendix Fig S4). Interestingly, we found that $dEsyt^{KO}$ did not enhance the reduced ERG amplitude resulting from the depletion of dPI4KIIIα (Appendix Fig S5), the enzyme implicated in the conversion of PI to PI4P at the PM of photoreceptors (Balakrishnan *et al*, 2018). The reason for this is unclear; however, it indicates that the enhancement of $rdgB^{9}$ phenotypes by $dEsyt^{KO}$ is specific and not seen even in cells depleted of the immediate next component of the PIP_2 cycle in photoreceptors. These findings strongly indicate a key role for dEsyt in specifically supporting the function of RDGB at the ER-PM MCS. Our data suggest that in photoreceptors with a full capacity of RDGB function, cells can dispense with the requirement for dEsyt. However, in cells with limiting RDGB function (such as $rdgB^{9}$), the requirement for dEsyt function becomes apparent. Thus, our data clearly support a role for dEsyt in supporting the lipid transfer function of RDGB at ER-PM contact sites *in vivo*. Consistent with this model, we found that the dEsyt protein is localized to the base of the microvillar PM at the ER-PM contact site where the RDGB protein is also specifically localized (Vihtelic *et al*, 1993; Yadav *et al*, 2018).

Although we found a normal density of ER-PM MCS in $dEsyt^{KO}$ photoreceptors at eclosion, we noted that this changed as a function of age and illumination. Wild-type photoreceptors show a reduction in ER-PM MCS density with age; however, the drop in MCS density under the same conditions was much greater in $dEsyt^{KO}$ with

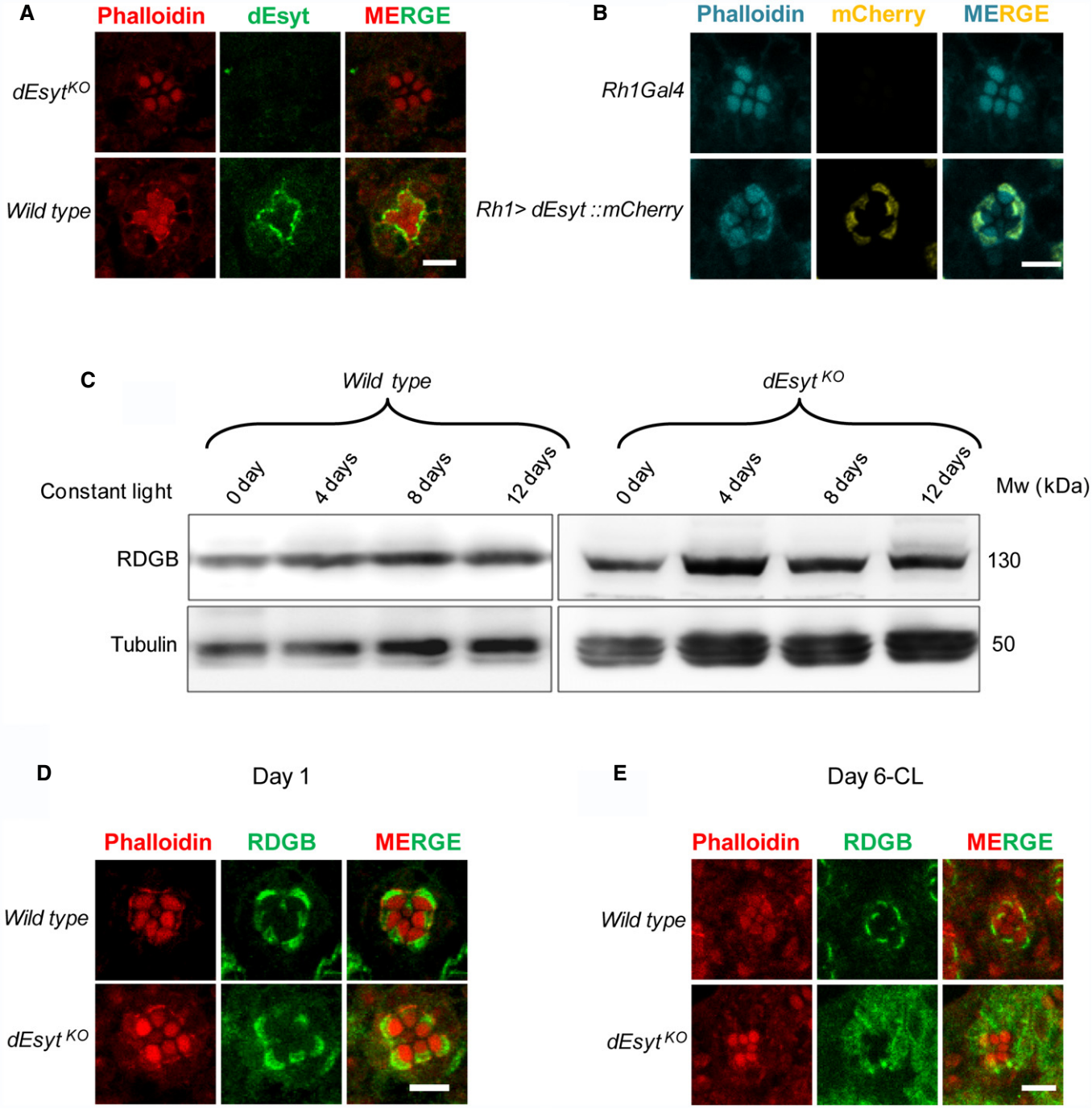

Figure 4. dEsyt localizes to MCS and determines RDGB localization.

A Confocal images showing the localization of endogenous dEsyt protein in photoreceptors of one-day-old dark-reared flies probed with antibody against dEsyt. Scale bar: 5 μm. *dEsyt*^{KO} shows no staining when probed with dEsyt antibody.

B Confocal images showing the localization of exogenously expressed dEsyt::mCherry protein expressed using the eye-specific Rh1-Gal4 in one-day-old dark-reared flies. Rh1-Gal4 is shown as a control. A single ommatidium is shown. Scale bar: 5 μm. Phalloidin marks F-actin staining and highlights rhabdomeres R1–R7.

C Western blot from the head extracts of wild type and *dEsyt*^{KO} probed with the antibody against RDGB. Rearing conditions, age of the flies, and genotype is indicated on top of the blot. Tubulin was used as the loading control.

D, E Confocal images showing the localization of RDGB in wild-type and *dEsyt*^{KO} photoreceptors of flies which are (D) 1-day-old dark-reared and (E) 6-day-old exposed to constant illumination. For (D) and (E) RDGB visualized using an antibody against the endogenous protein. Rhabdomeres are outlined using phalloidin which marks F-actin. Scale bar: 5 μm.

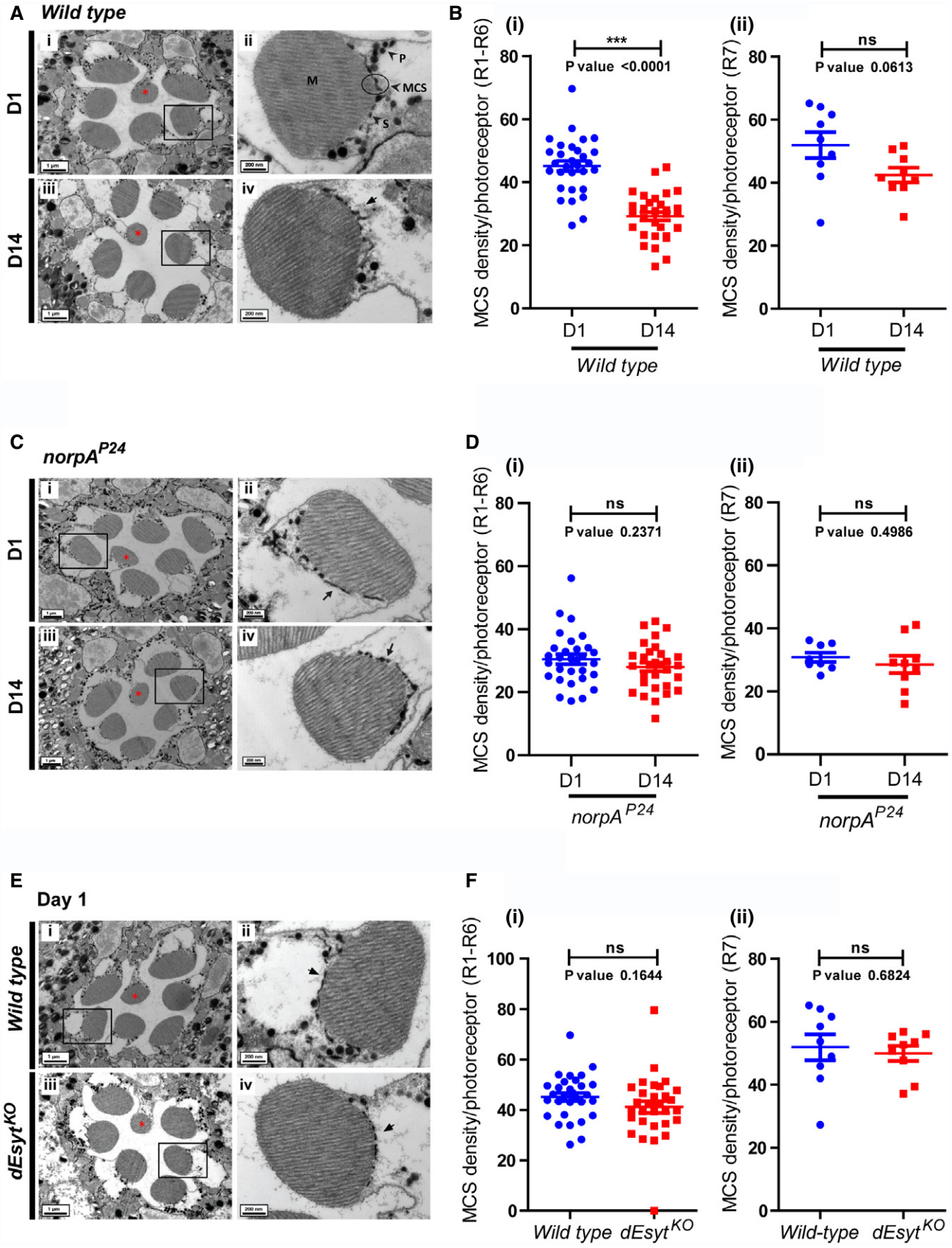

Figure 5.

Figure 5. dEsyt stabilizes MCS in photoreceptors.

A TEM images of a single ommatidium from wild-type photoreceptors of flies reared in dark (i) day 1 (D1) and (iii) day 14 (D14), scale bar: 1 μm (red asterisk indicates R7 photoreceptor). Magnified image showing a single photoreceptor from the same ommatidium (ii) day 1 (iv) day 14. Scale bar: 200 nm. Origin boxes for magnification shown. Arrow in (Aiv) indicates the SMC forming an MCS with the microvillar PM. M—microvillar plasma membrane, S—sub-microvillar cisternae, MCS—membrane contact site, P—pigment granules.

B Quantification of the number of MCS per wild-type photoreceptor of 1-day and 14-day-old flies reared in dark (from Fig 6A), *Y*-axis indicates the number of MCS/photoreceptor. n = 30 photoreceptors from 3 separate flies (R1–R6) for (i). n = 9 photoreceptors from 3 separate flies (R7) in (ii).

C TEM images of a single ommatidium from $norpA^{P24}$ photoreceptors of flies reared in dark (i) day 1 and (iii) day 14, scale bar: 1 μm (red asterisk indicates R7 photoreceptor). Magnified image showing a single photoreceptor from the same ommatidium (ii) day 1 (iv) day 14. Scale bar: 200 nm. Arrows indicate the SMC forming an MCS with the microvillar PM.

D Quantification of the number of MCSs per photoreceptor (from Fig 6C), *X*-axis indicates the genotype and age of the flies and *Y*-axis indicates the number of MCS/photoreceptor. (i) n = 30 photoreceptors from 3 separate flies (R1-R6). (ii) n = 9 photoreceptors from 3 separate flies (R7).

E TEM images of a single ommatidium from (i) wild-type and (iii) $dEsyt^{KO}$ photoreceptors of 0 to 1-day-old flies reared in dark, scale bar: 1 μm (red asterisk indicates R7 photoreceptor). (ii, iv) Magnified image showing a single photoreceptor from the ommatidium image shown on the left. Scale bar: 200 nm. Arrows indicate the SMC forming an MCS with the microvillar PM.

F Quantification of the number of MCS per photoreceptor of wild-type 1-day v/s $dEsyt^{KO}$ 1-day-old flies reared in dark, *X*-axis indicates the genotype and age of the flies and *Y*-axis indicates the number of MCS/photoreceptor. (i) n = 30 photoreceptors from 3 separate flies (R1-R6). (ii) n = 9 photoreceptors from 3 separate flies (R7).

Data information: Scatter plots with mean ± SD are shown. Statistical tests: (B, D, and F) Student's unpaired *t*-test. ns—Not significant; ***$P < 0.001$.

virtually no MCS observed in 14 days old, constant dark-reared flies. In addition to this, the overexpression of dEsyt specifically in the eye resulted in the recruitment of ER structures towards the apical PM with some part of the recruited structures invading the rhabdomere. This observation further supports a role dEsyt in supporting the positioning of the ER at the base of the microvilli and hence stabilizing MCS between the PM and ER at this location (Appendix Fig S6). Together, our observations imply that dEsyt function is essential to maintain the stability of ER-PM MCS in photoreceptors. We also observed that although the RDGB protein was correctly localized at the MCS at eclosion, in $dEsyt^{KO}$ photoreceptors, the protein became delocalized as a function of age in the absence of dEsyt function. By day 6, the RDGB protein was substantially delocalized from the base of the microvilli in $dEsyt^{KO}$, although the total amount of RDGB protein in the cell was not reduced. During this study, we also noted that the MCS density was lower in $rdgB^{9}$;$dEsyt^{KO}$ compared to $rdgB^{9}$ alone. This observation offers an explanation for the ability of $dEsyt^{KO}$ to enhance the physiological phenotypes of $rdgB^{9}$ on day 1 post-eclosion; i.e, the reduced MCS density in $rdgB^{9}$ with limited lipid transfer activity is further compromised by the additional loss of MCS resulting from $dEsyt^{KO}$. Taken together, these findings suggest that in the absence of dEsyt function, it is likely that RDGB (and perhaps other MCS localized proteins) become delocalized leading to disruption of its lipid transfer function. These findings lead us to a model of dEsyt function in photoreceptors where its key role is to stabilize ER-PM MCS and facilitate the correct localization of relevant proteins at this MCS.

Despite intense interest in the function of MCS, very little is known about the mechanisms by which MCS density is tuned in response to signals. In photoreceptors, a key signal is light and this is transduced through G protein-coupled PLCβ activity (reviewed in ref. Raghu *et al*, 2012). In this study, we made several observations that link MCS density to PLCβ activity: (i) In newly eclosed flies, MCS density was reduced in *norpA* mutants that lack PLCβ activity, (ii) in wild-type photoreceptors, ER-PM MCS density decreased as a function of age and this decrease was dependent on ongoing PLCβ activity, and (iii) the loss of MCS in $dEsyt^{KO}$ photoreceptors could be suppressed by *norpA* mutants. Together, these findings suggest that PLCβ activity is a key element of the mechanism by which MCS density is regulated. Interestingly, in $rdgB^{9}$, in which PM PIP_2 levels are lower than wild type, MCS density was reduced. Since both PLCβ and RDGB regulate PIP_2 levels, our observations suggest that MCS density in photoreceptors is modulated by PIP_2 turnover at the PM. As PIP_2 turnover is a key step of phototransduction in *Drosophila* photoreceptors, it is possible that in this cell type, illumination modulates MCS density. In turn, this will alter the biochemical activity of proteins localized at the MCS and their ability to maintain microvillar PM homeostasis. Future studies will likely reveal the molecular mechanism by which MCS density is tuned to ambient illumination and the broader question of PM homeostasis by MCS in eukaryotic cells.

Materials and Methods

Fly stocks

Flies (*Drosophila melanogaster*) were raised on rich medium (composition : corn flour, black jaggery, agar, dry yeast, propionic acid, methyl para hydroxy benzoate, orthophosphoric acid) at 25°C maintaining 50% relative humidity in a constant temperature laboratory incubator. The environment within the incubator was completely devoid of illumination except for the brief pulses of light to which the flies were subjected when the incubator doors were opened. The experiments were carried out in three different conditions: constant illumination, constant dark and 12-h light–dark cycle. For experiments involving constant illumination and 12-h light–dark cycle, incubators were maintained at 25°C with a white light source (light intensity: 8,000 lux) for the required time period. For constant dark rearing, flies within the vials were kept in tightly closed dark boxes and maintained in the constant temperature laboratory incubator. Gal4-UAS system was used for the selective activation of the transgene spatially and temporally for targeted gene expression.

Sequence and phylogeny analysis

The protein sequences for sequence alignment were obtained from NCBI: *Drosophila melanogaster*: dEsyt-PA (NP_733010.1), *Homo*

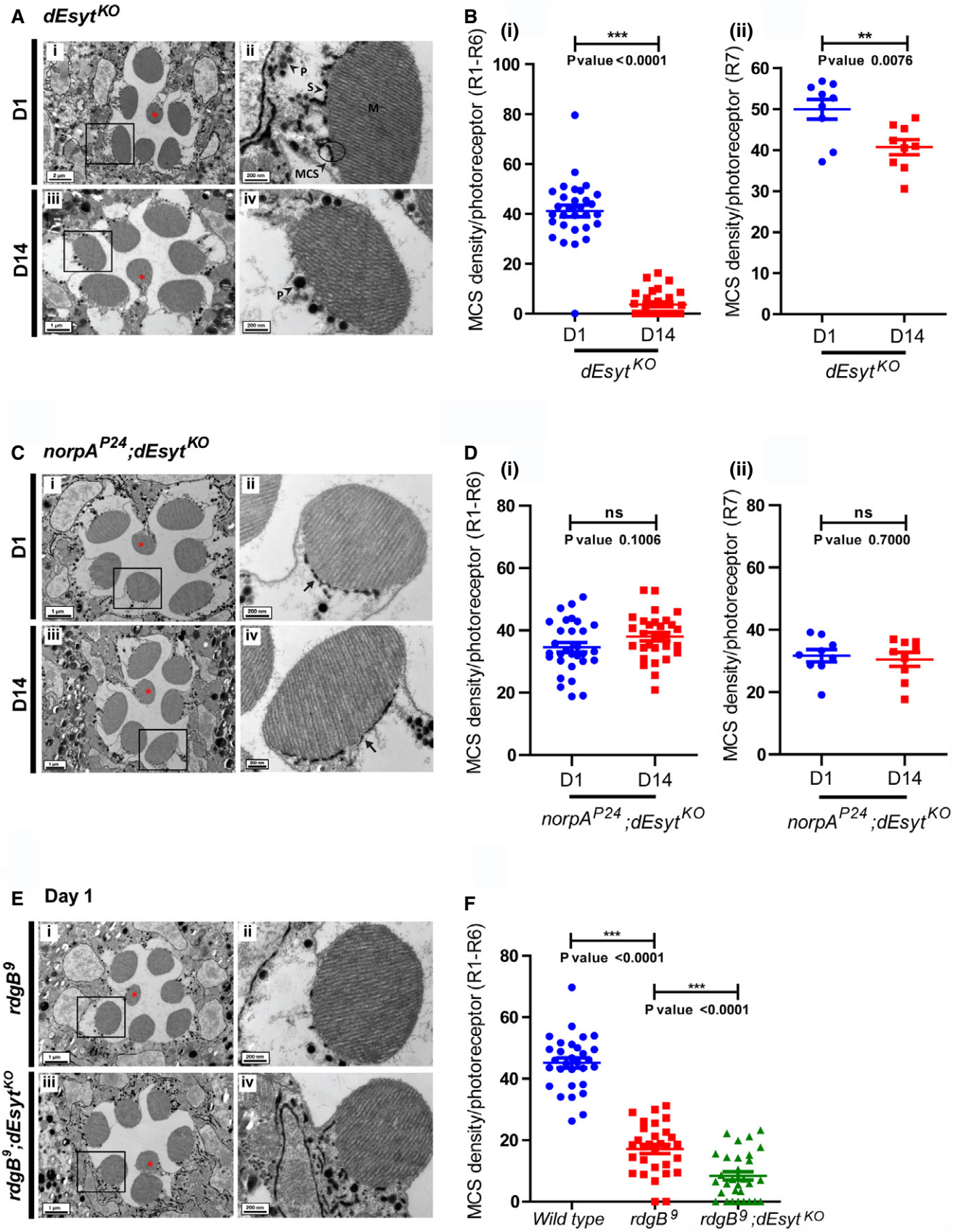

Figure 6.

Figure 6. dEsyt is necessary for PLCβ-dependent modulation of ER-PM MCS.

A TEM images of a single ommatidium from photoreceptors of (i) $dEsyt^{KO}$-day 1 (iii) $dEsyt^{KO}$-day 14 flies reared in dark, scale bar: 1 μm except for (Ai): 2 μm (red asterisk indicates R7 photoreceptor). (A-ii, iv) Magnified image showing a single photoreceptor from the ommatidium image shown on the left. Scale bar: 200 nm. Boxes represent the origin boxes for magnification. M—microvillar plasma membrane, S—sub-microvillar cisternae, MCS—membrane contact site, P—pigment granules.

B Quantification of the number of MCS per photoreceptor, *X*-axis indicates the genotype and age of the flies and *Y*-axis indicates the number of MCS/photoreceptor. $n = 9$ photoreceptors from 3 separate flies for R7.

C TEM images of a single ommatidium from photoreceptors of (i) $norpA^{P24}$;$dEsyt^{KO}$-day 1 (iii) $norpA^{P24}$;$dEsyt^{KO}$-day 14 flies reared in dark, scale bar: 1 μm (red asterisk indicates R7 photoreceptor). (C-ii, iv) Magnified image showing a single photoreceptor from the ommatidium image shown on the left. Scale bar: 200 nm. Arrows indicate the SMC forming an MCS with the microvillar PM.

D Quantification of the number of MCS per photoreceptor, *X*-axis indicates the genotype and age of the flies and *Y*-axis indicates the number of MCS/photoreceptor. (i) $n = 30$ photoreceptors from 3 separate flies for R1–R6. (ii) $n = 9$ photoreceptors from 3 separate flies for R7.

E TEM images of a single ommatidium from photoreceptors of (i) $rdgB^{9}$-day 1 and (iii) $rdgB^{9}$;$dEsyt^{KO}$-day 1 flies reared in dark, scale bar: 1 μm (red asterisk indicates R7 photoreceptor). (E-ii, iv) Magnified image showing a single photoreceptor from the ommatidium image shown on the left. Scale bar: 200 nm.

F Quantification of the number of MCS per photoreceptor for R1-R6 in 1-day-old dark-reared wild-type (from Fig 5B i), $rdgB^{9}$ and $rdgB^{9}$;$dEsyt^{KO}$ flies. $n = 30$ photoreceptors from 3 separate flies.

Data information: Scatter plots with mean ± SD are shown. Statistical tests: (B and D) Student's unpaired *t*-test. (F) One-way ANOVA with post hoc Tukey's multiple pairwise comparison. Ns—not significant, $^{**}P < 0.01$; $^{***}P < 0.001$.

sapiens: hEsyt1-isoform 1 (NP_001171725.1), hEsyt2-isoform 1 (NP_001354702.1), hEsyt3-isoform a (NP_001309760.1), *Saccharomyces cerevisiae*: yeast tcb1 (NP_014729.1), yeast tcb2 (NP_014312.1), yeast tcb3 (NP_013639.1), *Mus musculus*: Esyt1 Mm (NP_035973.1), Esyt2 Mm (NP_083007.2), Esyt3 Mm (NP_808443.2), *Rattus norvegicus*: Esyt1 Rn (NP_058945.2), Esyt2 Rn (NP_001258098.1), Esyt3 [Predicted (XP_343455.4)], *Xenopus tropicalis*: Esyt1 Xt (XP_002934579.1), Esyt2 Xt (XP_031759913.1), Esyt3 Xt (NP_001011364.1), *Danio rerio*: Esyt1a Dr (XP_695611.3), Esyt1b Dr (XP_699731.6), Esyt2a Dr (XP_005171454.1), Esyt2b Dr (XP_021333611.1), Esyt3 Dr (NP_001116705.1), and *Caenorhabditis elegans*: Esyt2 Ce (NP_741181.1). Multiple sequence alignment of dEsyt protein sequence with the human Esyts and yeast tricalbins were obtained using MUSCLE (MUltiple Sequence Comparison by Log-Expectation; Edgar, 2004). The phylogenetic tree reflecting the evolution of these proteins was obtained using neighbor-joining method MEGA6 (Molecular Evolutionary Genetics Analysis, version 6.0; Tamura *et al*, 2013).

Optical neutralization

The flies reared under experimental conditions were immobilized by cooling on ice, carefully decapitated, and fixed on the microscope slide using a drop of colorless nail varnish. The refractive index of the cornea was neutralized using a drop of immersion oil, viewed, and imaged under the 40× oil immersion objective of Olympus BX43 microscope. The digital image acquisition and documentation were done by using CellSens software.

Scoring retinal degeneration

To obtain a quantitative index of degeneration, a total of 50 ommatidia from 5 different flies of each genotype were assessed for each time point. The single, central UV-sensitive photoreceptor that did not show any light-dependent retinal degeneration was used as the reference and the rest of the photoreceptors were scored. A score of 1 was given to each rhabdomere that appeared to be wild type. Thus, the control photoreceptors will have a score of 7 and the mutants undergoing degeneration will have a score from 1 to 7. The results were analyzed, and the graph was plotted using GraphPad Prism software.

Electroretinogram

Anesthetized flies were introduced into truncated 200-μl disposable pipette tips such that the head protruded from the small opening. The fly's head was then immobilized using colorless nail varnish. Two glass microelectrodes (640786, Harvard Apparatus, Massachusetts, USA) filled with 0.8% NaCl solution were used for recordings such that the voltage changes were recorded by placing the experimental electrode on the surface of the eye and the reference electrode on the thorax. The flies were dark adapted for 5 min prior to ERG recordings followed by 2-s flash of green light stimulus, with 10 stimuli (flashes) per recording and 15 s of recovery time between two subsequent flashes. Green light stimulus was emitted using an LED light source to within 5 mm of fly's eye through a fiber optic guide. Voltage changes were recorded using pCLAMP 10.7 and amplified using DAM50 amplifier (SYS-DAM50, WPI, Florida, USA). Data analysis was done using Clampfit 10.7 (Molecular Devices, California, USA). Graphs were plotted using GraphPad Prism software.

Western blot

Age-matched flies were decapitated, and the heads were homogenized in 2× Laemmli sample buffer followed by boiling at 95°C for 5 min. For rhodopsin blot, the protein samples were processed differently. The fly heads were snap-frozen in liquid nitrogen and stored at −80°C for a period of 2 days. These head samples were homogenized in 2× Laemmli sample buffer followed by boiling at 37°C for 30 min. Protein extracts from fly heads were separated using SDS–PAGE and transferred onto nitrocellulose filter membrane [Hybond-C Extra; (GE Healthcare, Buckinghamshire, UK)] using wet transfer apparatus (Bio-Rad, California, USA). The membrane was blocked using 5% Blotto (sc-2325, Santa Cruz Biotechnology, Texas, USA) in phosphate buffer saline (PBS) with 0.1% Tween 20 (Sigma-Aldrich) (PBST) for 2 h at room temperature (RT). Primary antibody incubation was done overnight at 4°C using

appropriate antibody dilutions: anti-RDGB (lab generated), 1:1,000; anti-dEsyt (kind gift from Dr. Dion Dickman's lab), 1:2,000; anti-rhodopsin (4C5-DHSB, lowa, USA), 1:250; anti-Gq, 1:1,000; anti-TRP (lab generated), 1:4,000; anti-norpA, 1:1,000; and anti-α-tubulin-E7c (DHSB, lowa, USA), 1:4,000. Following this, the membrane was washed in PBST and incubated with 1:10,000 dilutions of appropriate secondary antibody (Jackson ImmunoResearch Laboratories, Pennsylvania, USA) coupled to horseradish peroxidase at RT for 2 h. Three PBST washes were given, and the blots were developed with ECL (GE Healthcare) and imaged using LAS 4000 instrument (GE Healthcare).

Fluorescent pseudopupil

To monitor changes in PIP_2 levels at the microvillar PM in live flies, the PIP_2 biosensor PH-PLCδ coupled to GFP driven by the transient receptor (*trp*) promoter of flies was used (Yadav *et al*, 2015). The flies were made insentient and were immobilized using the same protocol as in ERG recordings. The pseudopupil formed from the summed fluorescence of approximately 20–40 adjacent ommatidia were focused and imaged using the 10× objective of Olympus IX71 microscope. The program created using the software Micromanager captured time-lapse images of the pseudopupil by collecting fluorescence emitted from the eye when GFP was stimulated by a 90-ms flash of blue light. Prior to the recordings, the flies were dark adapted (resting conditions) for 6 min during which the probe binds to PIP_2 and localizes to the microvillar PM. Following a flash of blue light, the PLCβ activity triggers the hydrolysis of PIP_2, and thereby, the probe is displaced from the PM and this leads to the loss of the pseudopupil. The central UV-sensitive photoreceptor is unresponsive to blue light and thereby retains the probe at the apical PM. Subsequent red light illuminations following the blue light stimulus after each time-lapse image acquisition hastens the retrieval of the probe back to the PM. Mean fluorescence intensity indicating the basal PIP_2 pools and the PIP_2 recovery kinetics were calculated using ImageJ from NIH (Bethesda, MD, USA). Quantification of DPP fluorescence intensity was done by measuring the intensity values per area of the pseudopupil.

Similarly, flies expressing the P4M-GFP probe (PI4P biosensor) were subjected to the same protocol for monitoring PI4P levels. P4M-GFP expression was driven by an eye-specific promoter GMR using Gal4-UAS system.

RNA extraction and qPCR

RNA isolation was done from *Drosophila* heads using TRIzol reagent (Invitrogen) followed by treatment with amplification grade DNAse I (Invitrogen). cDNA synthesis was done using the Superscript II RNAse H Reverse Transcriptase (Invitrogen) and random hexamers (Applied biosystems). dEsyt primers were designed at the exon–exon junction of the dEsyt genomic region satisfying the parameters recommended for qPCR primer designing, and the run was performed in the Applied Biosystem7500 Fast Real Time PCR instrument using Ribosomal Protein 49 (RP49) primers as the control primers flanking the housekeeping gene region. Triplicates of each sample were measured to ensure the consistency of the data. The primers used for qPCR include the following:

RP49 forward: CGGATCGATATGCTAAGCTGT
RP49 reverse: GCGCTTGTTCGATCCGTA
dEsyt forward: GTTGTGGATAGTTGGCTCACCTT
dEsyt reverse: GCCTGGCTGAATCGATGAATAC
U6.1 forward: GATCCTGTGGCGGCTAC
U6.1 reverse: GAGGTGGAGTCTGGAAAGC

Immunohistochemistry

Retinae were dissected in PBS and fixed with 4% paraformaldehyde in PBS with 1 mg/ml saponin at room temperature for 30 min. Post-fixation, the samples were washed in PBS with 0.3% Triton X-100 (0.3% PBTX) followed by incubation with blocking solution (5% fetal bovine solution in PBTX) for 2 h at RT. The samples were then incubated overnight with the respective antibody [anti-RDGB (lab generated); 1:300, dEsyt (kind gift from Dr. Dion Dickman's lab); 1:200, mCherry (Thermo Fisher Scientific-PA5-34974); 1:300] at 4°C. After this, samples were washed thrice with 0.3% PBTX and incubated with appropriate secondary antibody [Alexa Fluor 488 anti-rabbit (A11034), anti-rat (A11006) and Alexa Fluor 633 anti-rabbit (A21070), Molecular Probes; 1:300 dilution] for 4 h at RT. Along with the secondary antibody incubation, Alexa Fluor 568–Phalloidin (Invitrogen, A12380; 1:300) was used to mark F-actin. Samples were washed thrice with 0.3% PBTX, followed by one final wash in PBS and were mounted with 70% glycerol in 1× PBS. The whole-mounted preparations were imaged under 60 × 1.4 NA objective, in Olympus FV 3000 microscope.

Electron microscopy

The fly heads of mentioned genotypes were cut and immersed in 2% osmium tetroxide, kept at 4°C for 1 h followed by incubation at 40°C for 4 days. Specimens were washed with distilled water, stained *enbloc* with uranyl acetate (0.5% in distilled water) for 3 h. After washing with distilled water, specimens were subjected to dehydration step and embedded in epon. Ultrathin sections of 60 nm were cut, and grids were subjected to poststaining with 2% uranyl acetate (in 70% ethanol) and Reynold's lead solution. Sections were imaged at 120 KV on a Tecnai G2 Spirit Bio-TWIN (FEI) electron microscope.

Scoring MCS density

For scoring MCS density/photoreceptor cell, a total of 30 cells were taken to conduct analysis for R1-R6 and 9 cells for R7. Using free-hand line tool of ImageJ, length of MCS (μm)/the total length of the base of the rhabdomere (μm) was calculated. Fractions of MCS coverage were multiplied with 100 to show the percentage. Groups were compared using the GraphPad Prism 8 software.

Statistical analysis

Unpaired two-tailed *t*-test or ANOVA, followed by Tukey's multiple comparison test, were carried out where applicable.

Data availability

No data were deposited in any public database.

Expanded View for this article is available online.

Acknowledgements

This work was supported by the Department of Atomic Energy, Government of India, under project no. 12-R&D-TFR-5.04-08002 and 12-R&D-TFR-5.04-0900, a Wellcome-DBT India Alliance Senior Fellowship (IA/S/14/2/501540) to PR, a Wellcome-DBT India Alliance Early Career Fellowship (IA/E/17/1/503653) to SM and the Department of Biotechnology, Government of India (BT/PRJ3748/GET/l 19/27/2015). We thank the *Drosophila* Facility, Central Imaging Facility and Electron Microscopy Facility at NCBS for support. We thank Dr. D. Dickman for sharing valuable reagents.

Author contributions

VRN and PR designed research; VRN, SM, and BB performed research; DT generated reagents; VRN, SM, and BB analyzed data; and VRN and PR wrote the paper.

Conflict of interest

The authors declare that they have no conflict of interest.

References

Balakrishnan SS, Basu U, Shinde D, Thakur R, Jaiswal M, Raghu P (2018) Regulation of PI4P levels by PI4KIIIα during G-protein-coupled PLC signaling in *Drosophila* photoreceptors. *J Cell Sci* 131: jcs217257

Balla T, Kim YJ, Alvarez-Prats A, Pemberton J (2019) Lipid dynamics at contact sites between the endoplasmic reticulum and other organelles. *Annu Rev Cell Dev Biol* 35: 85 – 109

Bian X, Saheki Y, De Camilli P (2018) ER-plasma membrane tethering with lipid transport. *EMBO J* 37: 219 – 234

Carrasco S, Meyer T (2011) STIM proteins and the endoplasmic reticulum-plasma membrane junctions *Annu Rev Biochem* 80: 973 – 1000

Chang C-L, Hsieh T-S, Yang TT, Rothberg KG, Azizoglu DB, Volk E, Liao J-C, Liou J (2013) Feedback regulation of receptor-induced Ca^{2+} signaling mediated by E-Syt1 and Nir2 at endoplasmic reticulum-plasma membrane junctions. *Cell Rep* 5: 813 – 825

Cockcroft S, Garner K, Yadav S, Gomez-Espinoza E, Raghu P (2016) RdgBα reciprocally transfers PA and PI at ER-PM contact sites to maintain PI(4,5)P_2 homoeostasis during phospholipase C signalling in *Drosophila* photoreceptors. *Biochem Soc Trans* 44: 286 – 292

Cockcroft S, Raghu P (2018) Phospholipid transport protein function at organelle contact sites. *Curr Opin Cell Biol* 53: 52 – 60

Edgar RC (2004) MUSCLE : multiple sequence alignment with high accuracy and high throughput. *Nucleic Acids Res* 32: 1792 – 1797

Gatta AT, Levine TP (2017) Piecing together the patchwork of contact sites. *Trends Cell Biol* 27: 214 – 229

Giordano F, Saheki Y, Idevall-Hagren O, Colombo SF, Pirruccello M, Milosevic I, Gracheva EO, Bagriantsev SN, Borgese N, De Camilli P (2013) PI(4,5)P_2-dependent and Ca^{2+}-regulated ER-PM interactions mediated by the extended synaptotagmins. *Cell* 153: 1494 – 1509

Hayashi M, Raimondi A, Toole EO, Paradise S, Collesi C, Cremona O, Ferguson SM, De Camilli P (2008) Cell- and stimulus-dependent heterogeneity of synaptic vesicle endocytic recycling mechanisms revealed by studies of dynamin 1-null neurons. *Proc Natl Acad Sci USA* 105: 1 – 6

Hepler PK, Palevitz BA, Lancelle SA, Mccauley MM, Lichtscheidl I (1984) Cortical endoplasmic reticulum in plants. *J Cell Sci* 96: 355 – 373

Herdman C, Tremblay MG, Mishra PK, Moss T (2014) Loss of Extended Synaptotagmins ESyt2 and ESyt3 does not affect mouse development or viability, but in vitro cell migration and survival under stress are affected. *Cell Cycle* 13: 2616 – 2625

Idevall-hagren O, Lü A, Xie B, De Camilli P (2015) Triggered Ca^{2+} influx is required for extended membrane tethering. *EMBO J* 34: 2291 – 2305

Kikuma K, Li X, Kim D, Sutter D, Dickman DK (2017) Extended synaptotagmin localizes to presynaptic ER and promotes neurotransmission and synaptic growth in *Drosophila*. *Genetics* 207: 993 – 1006

Kondo S, Ueda R (2013) Highly improved gene targeting by germline-specific Cas9 expression in *Drosophila*. *Genetics* 195: 715 – 721

Liu W, Xie Y, Ma J, Luo X, Nie P, Zuo Z, Lahrmann U, Zhao Q, Zheng Y, Zhao Y *et al* (2015) IBS: an illustrator for the presentation and visualization of biological sequences. *Bioinformatics* 31: 3359 – 3361

Loewen CJR, Young BP, Tavassoli S, Levine TP (2007) Inheritance of cortical ER in yeast is required for normal septin organization. *J Cell Biol* 179: 467 – 483

Manford AG, Stefan CJ, Yuan HL, MacGurn JA, Emr SD (2012) ER-to-plasma membrane tethering proteins regulate cell signaling and ER morphology. *Dev Cell* 23: 1129 – 1140

Matsumoto-Suzuki E, Hirosawa K, Hotta Y (1989) Structure of the subrhabdomeric cisternae in the photoreceptor cells of *Drosophila* melanogaster. *J Neurocytol* 18: 87 – 93

Omnus DJ, Manford AG, Bader JM, Emr SD, Stefan CJ (2016) Phosphoinositide kinase signaling controls ER-PM cross-talk. *Mol Biol Cell* 27: 1170 – 1180

Palade GE, Porter KR (1957) Studies on the endoplasmic reticulum: Its form and distribution in striated muscle cells. *J Biophys Biochem Cytol* 3: 269 – 300

Pearn MT, Randall LL, Shortridge RD, Burg MG, Pak WL (1996) Molecular, biochemical, and electrophysiological characterization of *Drosophila norpA* mutants. *J Biol Chem* 271: 4937 – 4945

Pichler H, Gaigg B, Hrastnik C, Achleitner G, Kohlwein SD, Daum È (2001) A subfraction of the yeast endoplasmic reticulum associates with the plasma membrane and has a high capacity to synthesize lipids. *Eur J Biochem* 268: 2351 – 2361

Raghu P, Yadav S, Mallampati NBN (2012) Lipid signaling in *Drosophila* photoreceptors. *Biochim Biophys Acta* 1821: 1154 – 1165

Roederer K, Cozy L, Anderson J, Kumar JP (2005) Novel dominant-negative mutation within the six domain of the conserved eye specification genesine oculis inhibits eye development in *Drosophila*. *Dev Dyn* 232: 753 – 766

Saheki Y, Bian X, Schauder CM, Sawaki Y, Surma MA, Klose C, Pincet F, Reinisch KM, De Camilli P (2016) Control of plasma membrane lipid homeostasis by the extended synaptotagmins. *Nat Cell Biol* 18: 504 – 515

Saheki Y, De Camilli P (2017) Endoplasmic reticulum-plasma membrane contact sites. *Annu Rev Biochem* 86: 659 – 684

Schauder CM, Wu X, Saheki Y, Narayanaswamy P, Torta F, Wenk MR, De Camilli P, Reinisch KM (2014) Structure of a lipid-bound extended synaptotagmin indicates a role in lipid transfer. *Nature* 510: 552 – 555

Sclip A, Bacaj T, Giam LR, Südhof TC (2016) Extended synaptotagmin (ESyt) triple knock- out mice are viable and fertile without obvious endoplasmic reticulum dysfunction. *PLoS One* 11: 1 – 17

Stefan CJ, Manford AG, Baird D, Yamada-Hanff J, Mao Y, Emr SD (2011) Osh proteins regulate phosphoinositide metabolism at ER-plasma membrane contact sites. *Cell* 144: 389 – 401

Suzuki E, Hirosawa K (1994) Immunolocalization of a *Drosophila* phosphatidylinositol transfer protein (*rdgB*) in normal and *rdgA* mutant

photoreceptor cells with special reference to the subrhabdomeric cisternae. *J Electron Microsc* 189: 183 – 189

Tamura K, Stecher G, Peterson D, Filipski A, Kumar S (2013) MEGA6: molecular evolutionary genetics analysis version 6.0. *Mol Biol Evol* 30: 2725 – 2729

Tremblay MG, Moss T (2016) Loss of all 3 Extended Synaptotagmins does not affect normal mouse development, viability or fertility. *Cell Cycle* 15: 2360 – 2366

Vihtelic TS, Goebl M, Milligan S, O'Tousa JE, Hyde DR (1993) Localization of *Drosophila* retinal degeneration B, a membrane-associated phosphatidylinositol transfer protein. *J Cell Biol* 122: 1013 – 1022

Yadav S, Garner K, Georgiev P, Li M, Gomez-Espinosa E, Panda A, Mathre S, Okkenhaug H, Cockcroft S, Raghu P (2015) RDGBα, a PtdIns-PtdOH transfer protein, regulates G-protein coupled PtdIns(4,5)P_2 signalling during *Drosophila* phototransduction. *J Cell Sci* 128: 3330 – 3344

Yadav S, Cockcroft S, Raghu P (2016) The *Drosophila* photoreceptor as a model system for studying signalling at membrane contact sites. *Biochem Soc Trans* 44: 447 – 451

Yadav S, Thakur R, Georgiev P, Deivasigamani S, Krishnan H, Ratnaparkhi G, Raghu P (2018) RDGBα localization and function at a membrane contact site is regulated by FFAT/VAP interactions. *J Cell Sci* 131: jcs207985

Yu H, Liu Y, Gulbranson DR, Paine A, Rathore SS, Shen J (2016) Extended synaptotagmins are Ca^{2+}-dependent lipid transfer proteins at membrane contact sites. *Proc Natl Acad Sci USA* 113: 4362 – 4367

